Supporting Information

Surface oxygen vacancy engineering on TiO_2 (101) via ALD technology for simultaneously enhancing charge separation and transfer

Wenbo Wu,[a] Zhenbo Peng,[b] Jun Wang,[a] Xiaoyu Li,[a] Ping Deng,[a] Yuhu Zhou,[a] Gan Jia,*[a] Wei Ye,*[a] and Peng Gao,*[a]

a. College of Material, Chemistry and Chemical Engineering, Hangzhou Normal University, Hangzhou, Zhejiang 311121, P. R. China.
b. Zhejiang Collaborative Innovation Center for High Value Utilization of Byproducts from Ethylene Project, Ningbo Polytechnic, Ningbo, Zhejiang 315800, P. R. China.
*Corresponding author
E-mail addresses: gjia@hznu.edu.cn (Gan Jia), yewei@hznu.edu.cn (Wei Ye), gaopeng@hrbeu.edu.cn (Peng Gao).

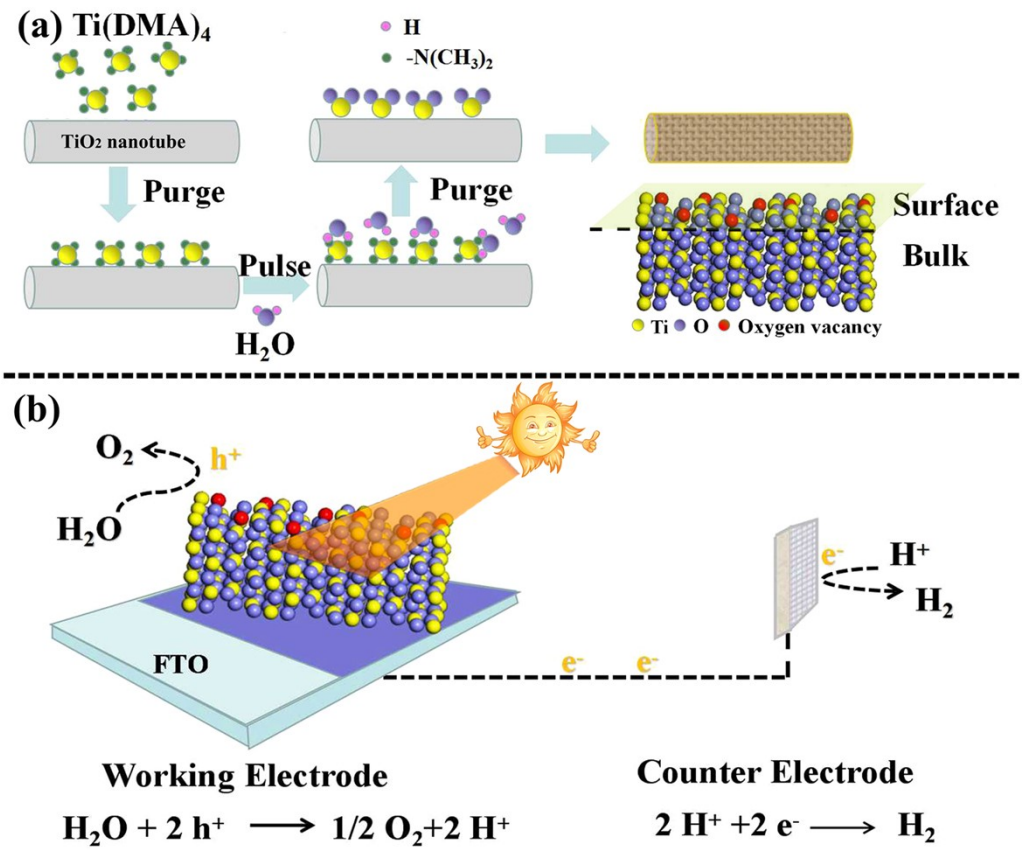

Scheme S1 Schematic illustration of the ALD process for surface oxygen vacancy construction (a) and the working mechanism of photoelectrode-based PEC water splitting (b).

Experimental section

Materials and Chemicals

All chemicals are of analytical grade and used without further purification, unless otherwise stated. All aqueous solutions were prepared to use deionized water with a resistivity of 18.25 MΩ.cm^{-1}. Tetrakis (dimethylamino) titanium (≥99.99%) was bought from Wuhan KLD Vacuum Technologies Co., Ltd, P25, NaOH (99%), EtOH (99.7%), HCl (36%), KOH (99.5%) and H_3BO_3 (99.5%) were purchased from Sinopharm Chemical Reagent. Ultrahigh-purity N_2 (99.999%), O_2 (99.999%), H_2 (99.999%) and compressed air (99.9%) were provided by Hangzhou Jingang Special Gas Co. Ltd.

Synthesis of TiO_2 nanotubes

TiO_2 nanotubes were prepared by hydrothermal reaction of P25 with an aqueous sodium hydroxide solution. 0.0125 mol of P25 was dispersed in a 40 mL 10 M aqueous sodium hydroxide solution. After stirring for 1 h at room temperature to fully dissolve, the solution was transferred to a 50 ml polytetrafluoroethylene-lined stainless steel autoclave and reacted at 135 °C for 24 h, followed by natural cooling to room temperature. The reaction products were first washed with distilled water and dried in a vacuum, and then acidified with 0.01 M hydrochloric acid solution for 6 h at room temperature, followed by vacuum drying at 70 °C for 12 h. Calcination in air transforms the synthesized sample into a pure titanium dioxide phase, allowing the sample product to be completely oxidized. The heating process was performed on a porcelain boat without any inert gas protection and was calcined for 5 hours at 500 °C (heating rate set to 5 °C/min). After calcination, the sample was cooled to room temperature, and the final product was anatase TiO_2 nanotubes.

Synthesis of titanium oxygen layer on titanium dioxide surface

The titanium oxygen layer grows on the surface of titanium dioxide at 200 °C. Alternating doses of TDMAT and H_2O pulsed using the timing sequence of t1-t2-t3-t4 (all times in s): corresponding to the pulse time of TDMAT, the purge time after the titanium pulse, the pulse time of H_2O, and the subsequent purge time after the H_2O pulse, respectively. TiO_x-N (N: 10–50 cycles), approximately 20 mg of TiO_2 was placed in a custom-made ALD powder sample holder. The sample was allowed to equilibrate for 30 min in the ALD sample chamber at 200°C with 7.8 sccm N_2 flow. The following timing sequence was used for titanium oxygen layer deposition: 0.2 s, 20 s, 0.015 s, 20 s. Samples with different surface oxygen vacancy concentrations were prepared by deposition with different cycles.

Preparation of TiO_x nanotubes photoanode

After ultrasonically cleaning in deionized water, acetone, and ethanol for 10 minutes in proper order, the fluorine-doped SnO_2 (FTO) glass pieces were used to prepare working electrodes. The slurry, which was prepared by 5 mg of photocatalyst ultrasonically dispersed into 0.7 ml ethyl alcohol and 0.3 ml deionized water for 1 hour, was drip-coated on the conductive surface of FTO glass to form a uniform photocatalyst film with an area of 1 cm^2. A catalyst-coated FTO glass was used as the working electrode, a platinum sheet was used as the counter electrode, and a saturated Ag/AgCl was used as the reference electrode.

Characterization

With the help of X-ray powder diffraction (XRD, German Bruker D8-Advance diffractometer, Cu Kα1, λ=0.15405 nm), the crystalline phase of catalysts was characterized. The scanning range was 10–70°with a 5°min^{-1} scanning speed. Transmission electron microscopy (TEM, JEOLJEM-2100, Japan) was employed to observe the morphologies and microstructure of the obtained samples. A high-resolution transmission electron microscope (HRTEM, JEM-2100) was used to observe the morphology of the prepared samples at 200 kV. The field emission scanning electron microscopy (FESEM) images and energy dispersive X-ray spectrum (EDS) were taken on a SU8000 cold emission field scanning electron microanalyzer (Hitachi, Japan). Transmission electron microscopy (TEM, JEOLJEM-2100, Japan) was employed to observe the morphologies and microstructure of the obtained samples. A high-resolution transmission electron microscope (HRTEM, JEM-2100) was used to observe the morphology of the prepared samples at 200 kV. Raman spectrometer (Renishaw inVia) was used with a working power of 50 mW, and an accumulation time of 30 s under 532 nm excitation wavelength. FT-IR spectra were recorded on a Perkin-Elmer 580B IR spectrophotometer using the KBr pellet technique. The electron spin resonance (EPR) spectra of the samples were recorded by a Bruker E500 spectrometer in the air at room temperature. Using $BaSO_4$ as the reference, the ultraviolet-visible diffuse reflectance spectra (DRS) of the photocatalysts were collected within a range of 200−800 nm by a UV-2600 UV/vis spectrophotometer. The band gap can be calculated using the following equation:

$$(\alpha h\nu)^{1/n} = A(h\nu - E_g) \quad \text{(S1)}$$

Where α, hυ and A represent absorption coefficient, photon energy, and absorption edge width parameters respectively. TiO_2 is an indirect semiconductor with an n value of 2.[1] Brunauer-Emmett-Teller (BET) nitrogen adsorption-desorption measurements were determined by Quadrasorb SI surface area and a pore size analyzer. Thermo-gravimetric analyses (TGA, Q500, TA Instruments USA) were performed in air and argon atmospheres with a heating rate of 10 °C/min from 30 to 800 °C. X-ray photoelectron spectroscopy (XPS, AXISULTRA) was employed to identify the chemical states of the surface compositions in a Kratos-Axis-Ultra system equipped with monochromatic Al Kα X-rays (1486.6 eV). Photoluminescence (PL) spectra of the as-obtained photocatalysts were recorded on a fluorescence spectrometer (JY HORIBA FluoroLog-3) under 380 nm excitation wavelength to research the separation efficiency of the photoinduced charge carriers. The fluorescence lifetimes of the

photocatalytic materials were obtained by using a FLUOROMAX-4 spectrophotometer at room temperature. The average fluorescence lifetime (τ_a) can be calculated using the following equation:

$$\tau_a = (A_1\tau_1^2 + A_2\tau_2^2)/(A_1\tau_1 + A_2\tau_2) \quad \text{(S2)}$$

Where τ_1 and τ_2 are the fluorescence lifetimes and A_1, and A_2 is the corresponding amplitudes.[2]

Photocatalytic H_2 evolution

Photocatalytic global water decomposition was carried out in a side-irradiated vessel connected to a glass gas circulation system. They were performed under different lighting conditions in the CEL-PEM-D6 online system (China Education AU-light Company Limited, Beijing). A 300 W xenon lamp (CEL-HXF100) was used as the incident light source, with an intensity of 100 mW /cm^2. In a typical photocatalytic total water decomposition reaction, 50 mg of the sample preparation and 5mL of methanol are dispersed in deionized water (50 mL) under constant magnetic agitation and top irradiation. The reaction system was irradiated for 1 hour after the air in the reaction slurry was completely removed by vacuuming. During the irradiation, the collected gas was analyzed by A GC-7920 gas chromatograph equipped with A thermal conductivity detector and 5 A molecular sieve column, N_2 as carrier gas.

Photoelectrochemical performances

Photoelectrochemical (PEC) performances of the TiO_x sample were measured using a typical three-electrode cell with a Xe 300 W lamp as the light source. The light was illuminated through an AM 1.5 G filter and the light intensity was carefully calibrated to ca. 100 mW cm^{-2} by a thermopile optical detector (Beijing Zhongjiao Jinyuan Co., LTD, CEL-NP2000). A platinum wire and an Ag/AgCl (saturated KCl) electrode were used as the counter electrode and reference electrode, respectively. A 1 M borate buffer solution was prepared by dissolving 0.1 mol of H_3BO_3 in 100 mL of Milli-Q water, followed by adding KOH to achieve a pH of 9.5, which was then used as the electrolyte for all PEC measurements, while the charge separation efficiencies of the samples were measured in the presence of 0.2 M Na_2SO_3 by keeping the pH at 9.5. Photocurrent-potential curves were obtained using LSV in a voltage window of 0.4~1.3 V versus RHE with a scan rate of 10 mV s^{-1} on an electrochemical workstation (CHI660E, CH Instruments, Inc.). The long-term stability of the photoanode was evaluated at 1.23 V versus RHE under AM 1.5 G illumination for 49 h with an interval of 3 h between each 10 h. To evaluate the overall water-splitting performance, the photocurrent densities of the TiO_x samples were measured in an air-tight cell at 1.23 V versus RHE under AM 1.5 G illumination for 5 h and the number of gases was detected with a gas chromatograph (SP7800, TCD, molecular sieve 0.5 nm, N_2 carrier, Beijing Keruida Limited) every 2 h. All the potentials versus RHE were converted from the potentials versus Ag/AgCl according to the Nernst equation:[3]

$$E_{RHE} = E_{Ag/AgCl} + 0.059 \times PH + E^0_{Ag/AgCl} \quad \text{(S3)}$$

Where E_{RHE} refers to the converted potential versus RHE. The value of $E^0_{Ag/AgCl}$ is 0.197 V at ambient temperature (25 °C) and $E_{Ag/AgCl}$ is the obtained potential versus Ag/AgCl. Applied bias photon-to-current efficiency (ABPE) can be calculated using the following equation:[4]

$$ABPE(\%) = \frac{J \times (1.23 - V_b)}{P_{total}} \quad \text{(S4)}$$

J is the photocurrent density (mA cm^{-2}) obtained from the electrochemical workstation. V_b refers to the applied bias versus RHE (V), and P_{total} is the total light intensity of AM 1.5 G (100 mV cm^{-2}).

Incident-photon-to-current conversion efficiency (IPCE) was obtained using a monochromator coupled with a 300

W Xe lamp as the simulated light source. An applied potential of 1.23 V versus RHE was supplied by a CHI 660d electrochemical workstation and the power density at a specific wavelength was measured by a Newport 1918-c power meter. IPCE values were calculated using Equation S5.[4]

$$IPCE(\%) = \frac{J \times 1240}{\lambda \times P_{light}} \times 100\% \quad \text{(S5)}$$

Where J presents the photocurrent density (mA cm^{-2}) obtained from the electrochemical workstation. λ and P_{light} are the incident light wavelength (nm) and the power density obtained at a specific wavelength (mW cm^{-2}), respectively.

Electrochemical impedance spectroscopy (EIS) spectra were collected with an AC voltage amplitude of 10 mV at the open circuit potentials of the samples under AM 1.5 G illumination (Frequency range: 0.01 Hz~100 kHz). Mott-Schottky (MS) spectra were obtained in the voltage window of 0~1.0 V versus RHE in the dark (increment: 10 mV, frequency: 1 kHz). According to the MS curves, the charge carrier density (N_d) can be calculated using the following equation:[5]

$$N_d = \frac{2}{e\varepsilon_0\varepsilon} \times d(\frac{1}{C^2}) / dv \quad \text{(S6)}$$

The electronic charge (e) is 1.6×10^{-19} C, vacuum permittivity (ε_0) is 8.86×10^{-12} F m^{-1}, and relative permittivity (ε) is 31 for TiO_2.[6] C (F cm^{-2}) is the space charge capacitance in the semiconductor (obtained from MS curves), and Vs (V) is the applied potential for MS curves.

The light harvesting efficiency (η_{LH}) of a semiconductor can be calculated using the following equation:[4]

$$\eta_{LH} = 1 - 10^{-A} \quad \text{(S7)}$$

The light absorbance (A) is measured experimentally by UV-vis spectroscopy. Charge separation efficiency (η_{sep}, the yield of photogenerated holes that have reached the semiconductor/electrolyte interfaces) and surface charge transfer efficiency (η_{trans}, the yield of holes that are involved in water oxidation reaction after reaching the electrode/electrolyte interfaces) of the TiO_2 and TiO_x samples, can be calculated using the following equations:[7]

$$\eta_{sep} = \frac{J^{Na_2SO_3}}{J_{abs}} \quad \text{(S8)}$$

$$\eta_{trans} = \frac{J^{H_2O}}{J^{Na_2SO_3}} \quad \text{(S9)}$$

J_{abs} is the unity converted photocurrent density from the light absorption, while J^{H_2O} and $J^{Na_2SO_3}$ are the photocurrent densities obtained in 1 M potassium borate electrolytes (pH 9.5) without and with 0.2 M Na_2SO_3, respectively.

Open circuit potentials of the photoanodes in dark and under AM 1.5 G illumination after stabilizing for 20 minutes with constant stirring were measured in 1 M potassium borate electrolytes (pH 9.5) without and with 0.2 M Na_2SO_3, respectively.

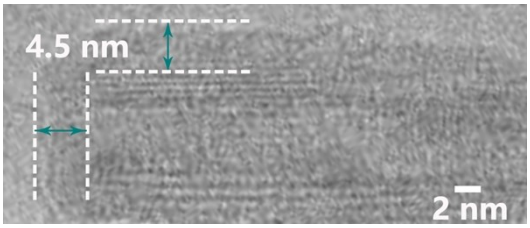

Fig. S1 HRTEM images of TiO_x after 200 cycles according to the as-used ALD parameters.

The thickness is ~ 4.5 nm measured by HRTEM and thus theoretical average deposition thickness of every cycle is 0.0225 nm, as shown in the HRTEM result.

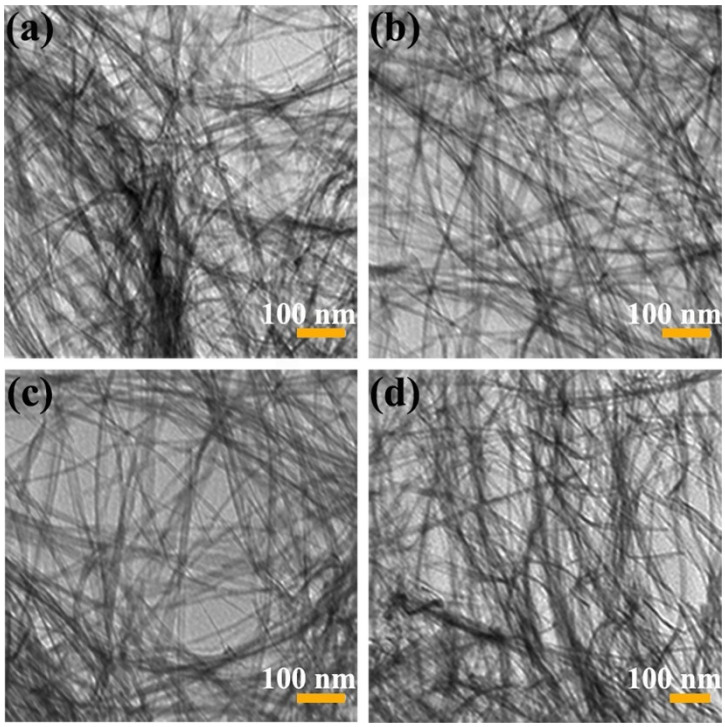

Fig. S2 TEM images of (a) TiO_x-10, (b) TiO_x-20, (c) TiO_x-30, (d) TiO_x-50, respectively.

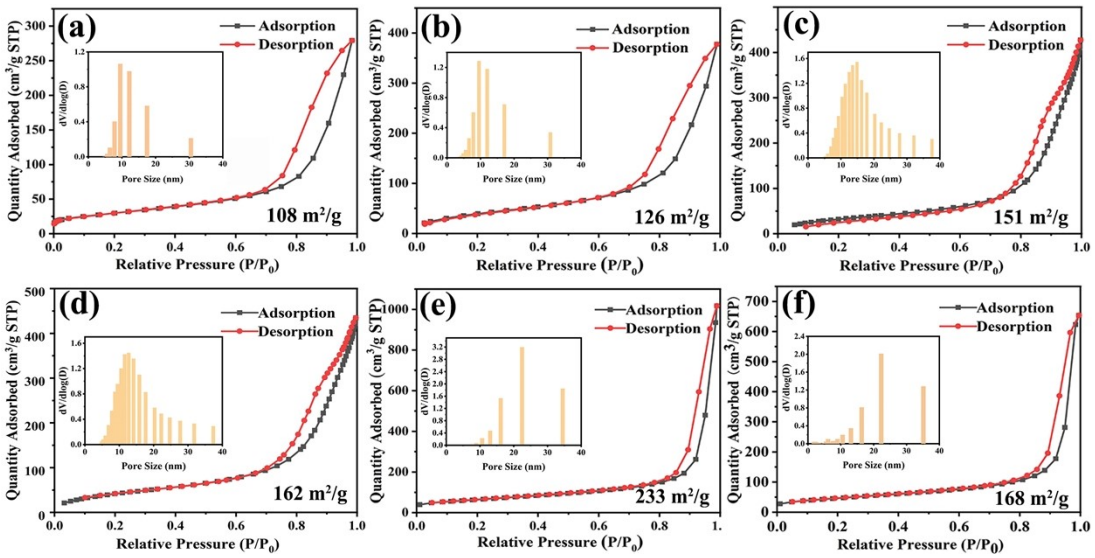

Fig. S3 Nitrogen adsorption-desorption isotherms of TiO_2 (a) and TiO_x-10, TiO_x-20, TiO_x-30, TiO_x-40, TiO_x-50 (b-f), respectively. (Inset: pore size distribution analysis of TiO_x samples based on their corresponding N_2 isotherms)

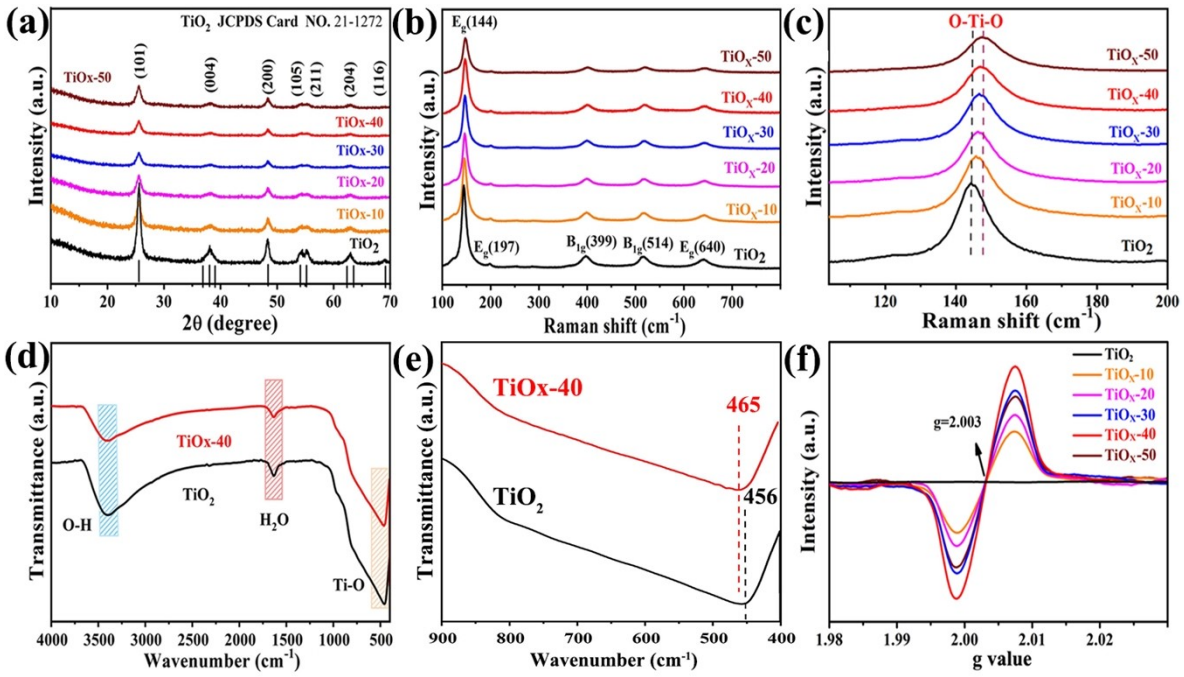

Fig. S4 (a) XRD patterns and (b) Raman spectra of TiO_2 and TiO_x. (c) Enlarged Raman patterns. (d) FI-IR spectra and (e) their selective amplification of TiO_2 precursor and the as-obtained TiO_x-40 sample. (f) EPR spectra of the samples with different ALD deposition cycles.

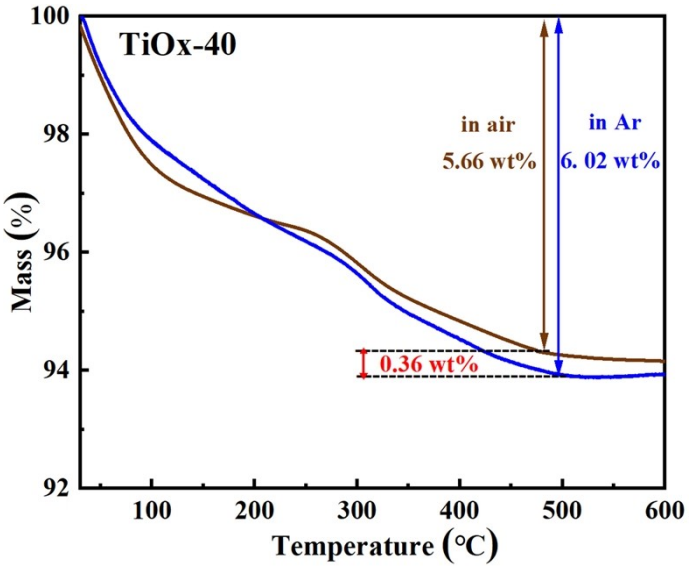

Fig. S5 TG curves of TiO_2 and TiO_x-40 in air and Ar atmosphere, respectively.

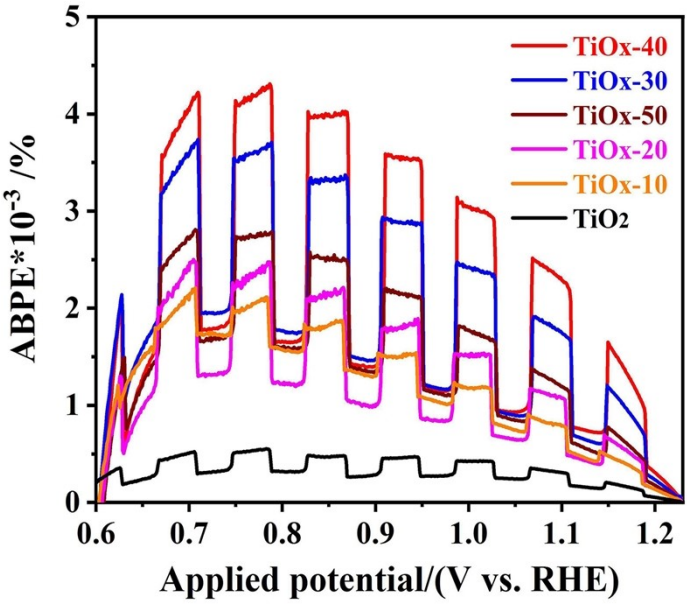

Fig. S6 ABPE curves of TiO_2 and TiO_x in a 1 M borate buffer electrolyte in the presence of 0.2 M Na_2SO_3 under AM 1.5 G illumination.

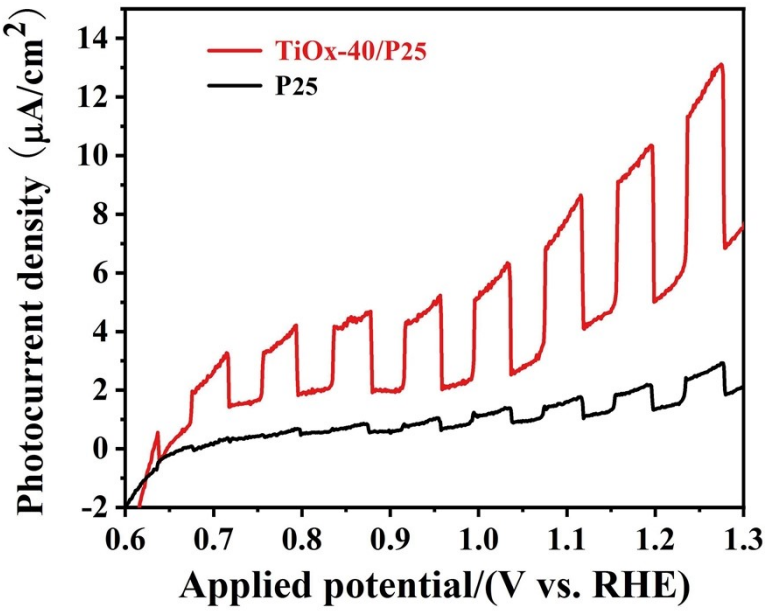

Fig. S7 Photocurrent density versus potential of P25 and TiO_x-40/P25 in a 1 M borate buffer electrolyte under AM 1.5 G illumination.

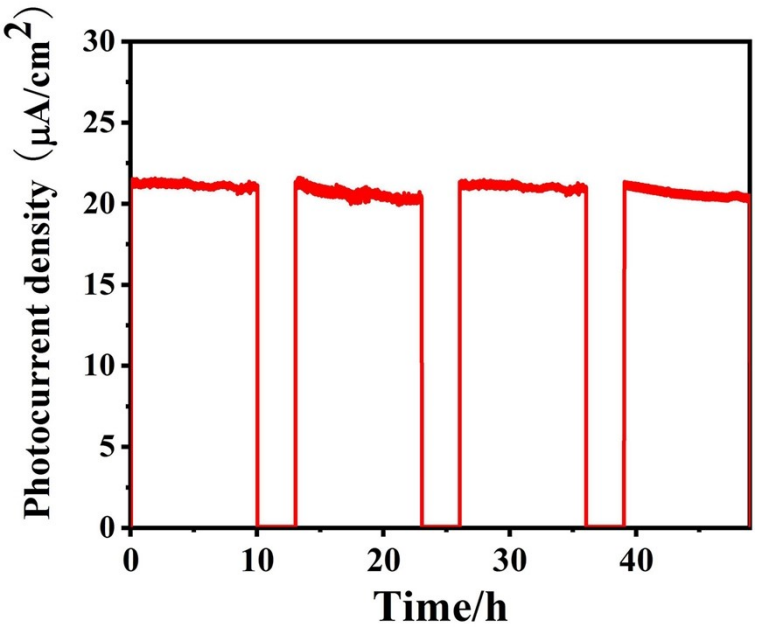

Fig. S8 J-t curve of the TiO_x-40 at 1.23 V versus RHE under AM 1.5 G illumination in a 1 M borate buffer electrolyte.

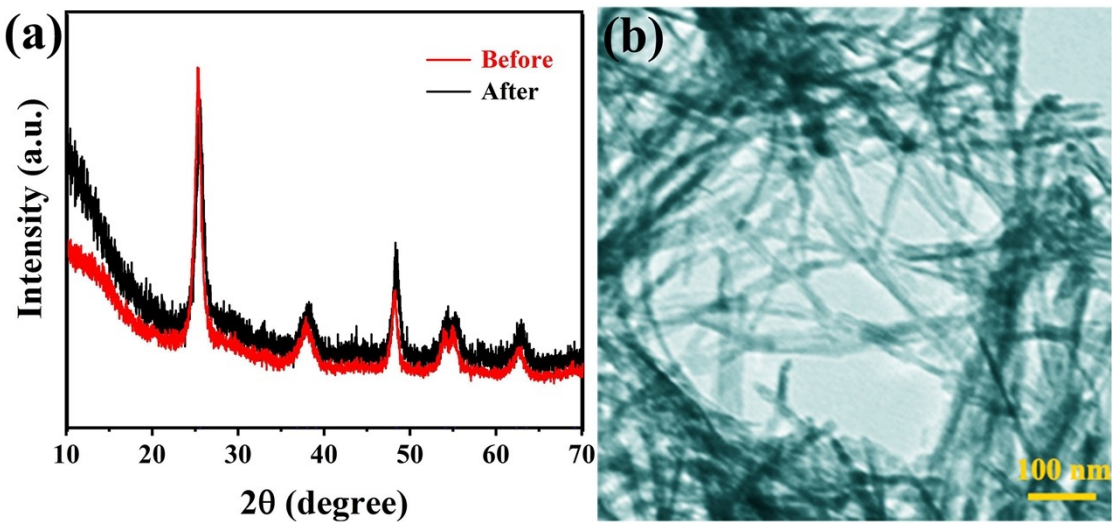

Fig. S9 (a) XRD patterns and (b) TEM images of TiO_x-40 photoanodes after a 49 hours long-term overall water splitting test.

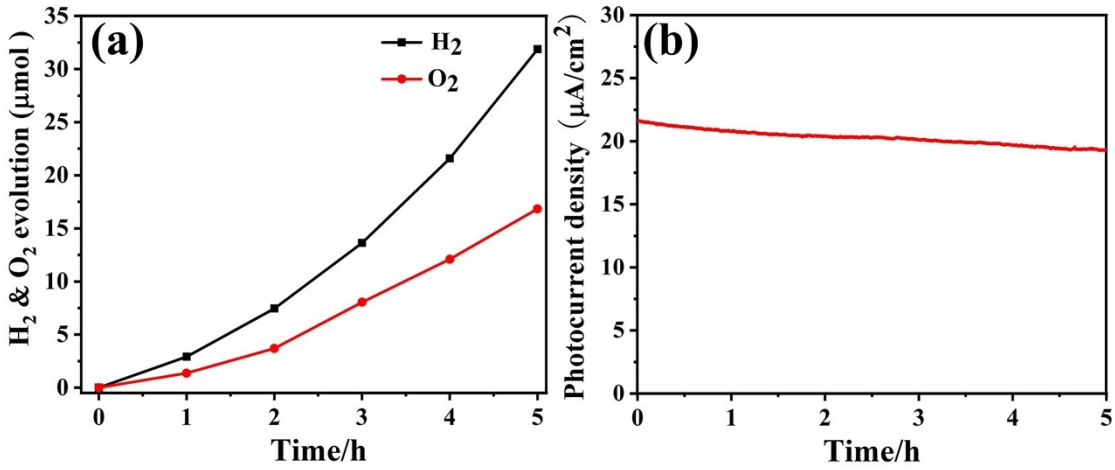

Fig. S10 (a) The corresponding H_2 and O_2 evolution performance. (b) J-t curve of the TiO_x-40 at 1.23 V versus RHE under AM 1.5 G illumination in a 1M borate buffer electrolyte.

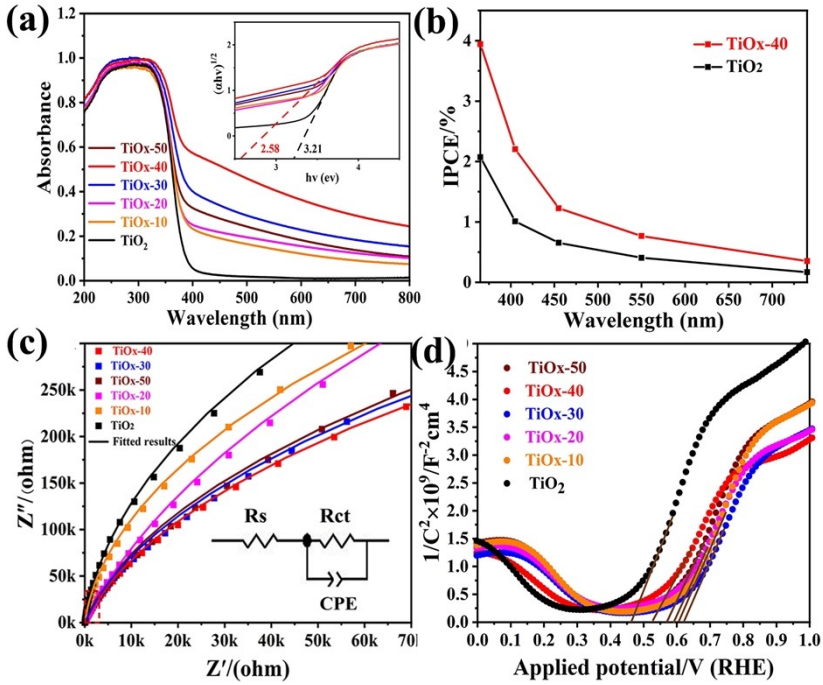

Fig. S11 (a) UV-Vis curves (Inset: the transformed Kubelka-Munk function versus the energy spectra). (b) IPCE curves. (c) EIS curves (Inset: the equivalent circuit model) at the open circuit potential under AM 1.5 G illumination. (d) MS curves under dark of TiO_2 and TiO_x. The measurements of (b-d) were performed in a 1 M borate buffer electrolyte (pH 9.5).

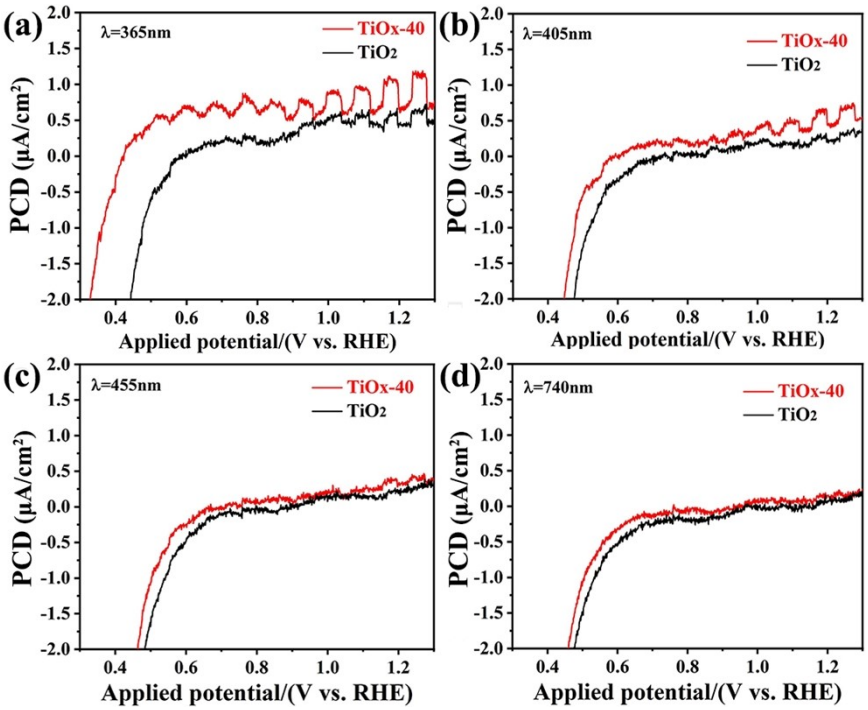

Fig. S12 Photocurrent density versus potential of TiO_2 and TiO_x-40 in a 1 M borate buffer electrolyte containing 0.2 M Na_2SO_3 under monochromater (the power density obtained at. 100 mW cm^{-2}).

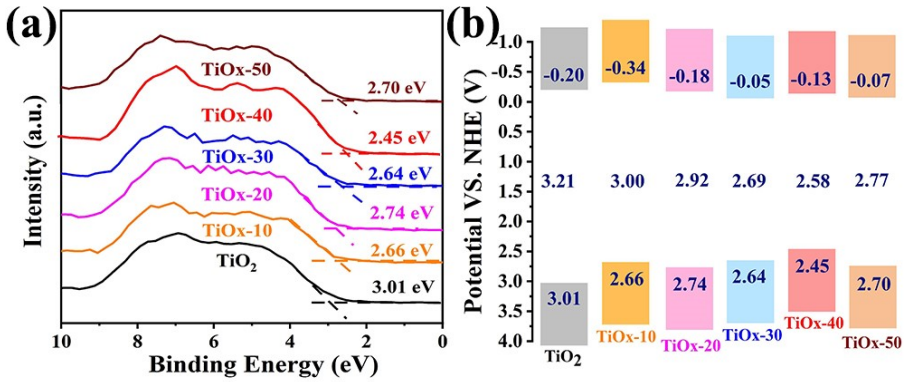

Fig. S13 (a) The valence bands of TiO_2 and TiO_x with different ALD deposition cycles. (b) The band gaps.

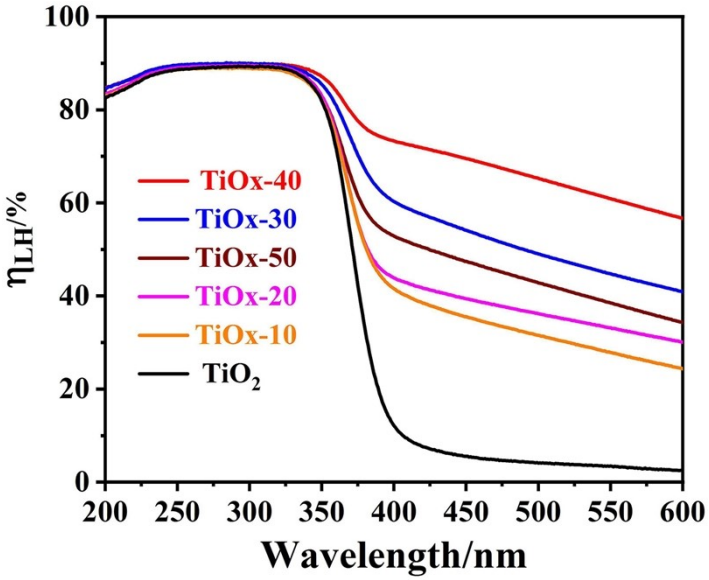

Fig. S14 η_{LH} curves of the TiO_2 and TiO_x samples.

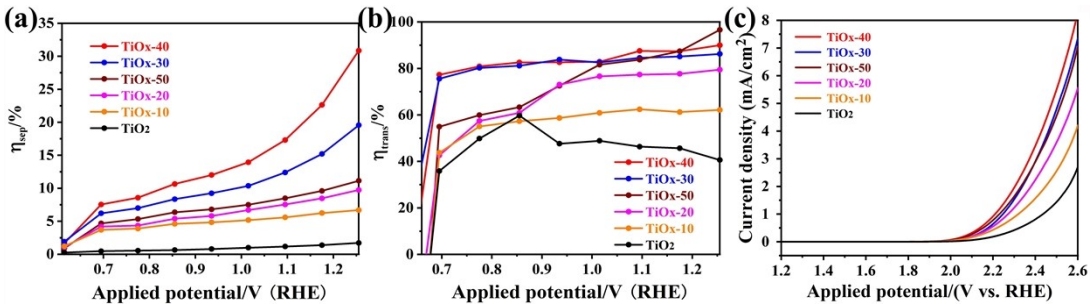

Fig. S15 (a) Charge separation efficiencies. (b) Charge transfer efficiencies. (c) Current density versus applied potential curves.

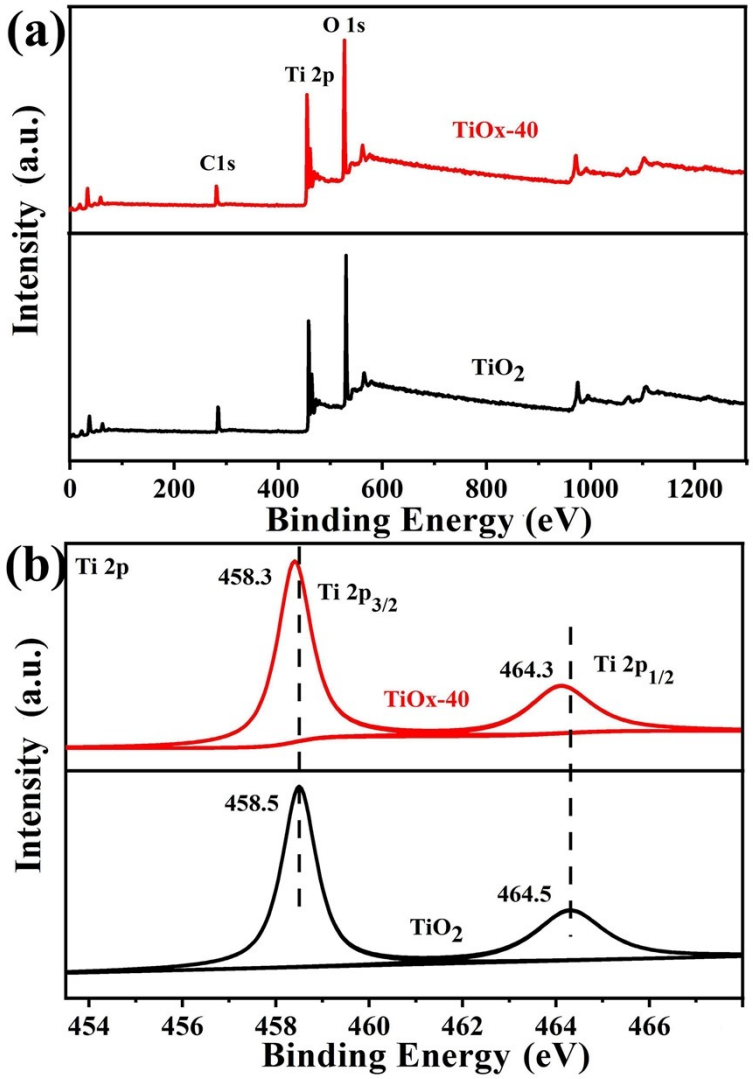

Fig. S16 (a) Full scan and (b) Ti 2p XPS spectra of TiO_x-40 and TiO_2.

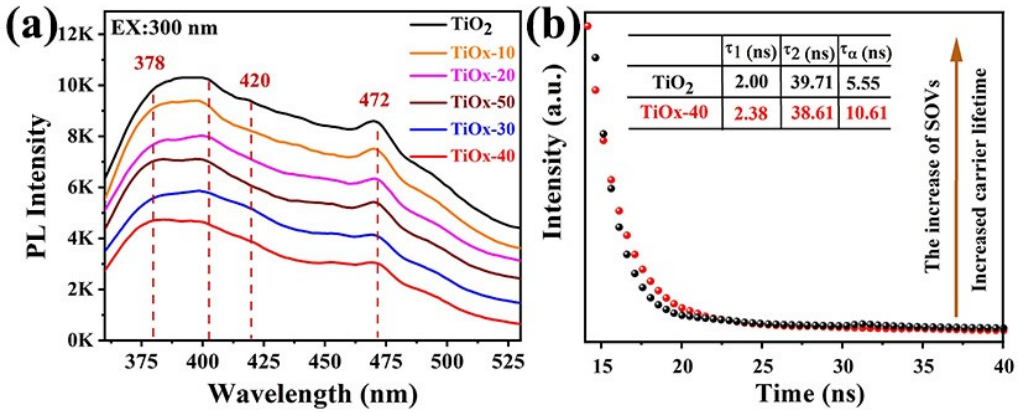

Fig. S17 (a) PL spectra excited by 300 nm. (b) Transient fluorescence spectra of TiO_2 and TiO_x-40 with an enhanced built-in electric field.

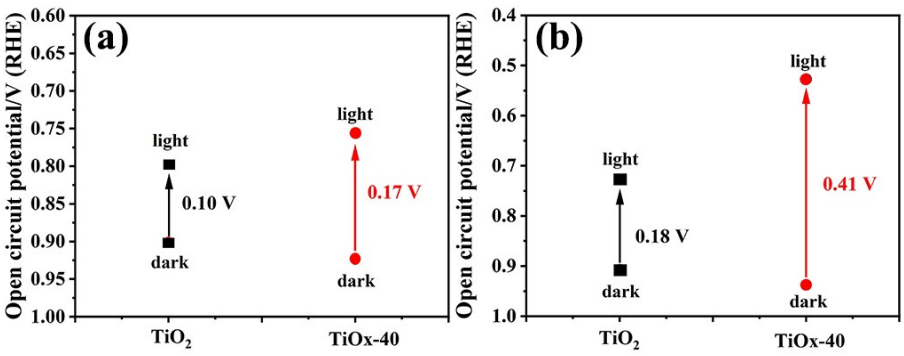

Fig. S18 (a) Open circuit potentials of the photoanodes in dark and under AM 1.5 G illumination of TiO_2 and TiO_x-40 after stabilizing for 20 min with constant stirring were measured in 1 M potassium borate electrolytes (pH 9.5) without and (b) with 0.2 M Na_2SO_3, respectively.

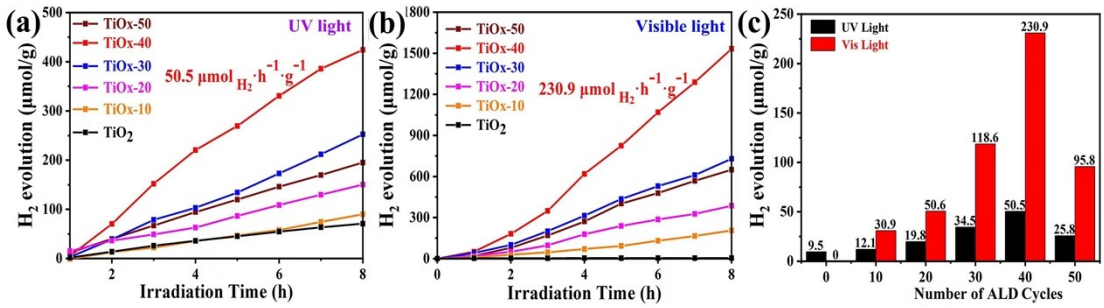

Fig. S19 Photocatalytic decomposition of water for hydrogen production: (a) under ultraviolet light, (b) under visible light. (c) H_2 generation activity under UV and visible light by various catalysts.

Table S1 Fitted results of the EIS curves in Fig. S11c.

Samples	Rct（MΩ）
TiO_2	2.87
TiO_x-10	2.39
TiO_x-20	2.02
TiO_x-30	1.31
TiO_x-40	1.26
TiO_x-50	1.46

Table S2 Carrier densities (N_d) of TiO_2 and TiO_x.

Samples	$Nd/10^{18}cm^{-2}$
TiO_2	2.75
TiO_x-10	3.20
TiO_x-20	3.27
TiO_x-30	3.64
TiO_x-40	4.13
TiO_x-50	3.31

Table S3 Comparison of charge separation efficiency (η_{sep}) and surface charge transfer efficiency (η_{trans}) in photoelectric chemical performance (AM 1.5 G, 100 mW/cm^2) between TiO_x and reported literature.

Photoanode	**η_{sep}**	**η_{trans}**	**Reference**
TiO_2	23%	/	**Nat. Commun.** 2020, 11, 2129
TiO_2	/	40%	**J. Energy Chem.** 2021, 60, 512.
$BiOI/TiO_2$	12%	43%	**Appl. Sure. Sci.** 2022, 601, 154277.
TiO_2/α-Fe_2O_3/ Cu:NiOx/CoPi	31.6%	59.6%	**ChemSusChem** 2021, 14, 2331
$BiVO_4/TiO_2$	38%	63%	**ACS Appl. Mater. Interfaces** 2021, 13, 60602
Sn-Fe_2O_3/TiO_2	12%	64%	**Chem. Eng. J.** 2019, 370, 314.
A-Fe_2O_3/ Au/TiO_2	18%	68%	**Appl. Catal. B: Environ.** 2020, 260, 118206.
Fe_2O_3/TiO_2	24.5%	73%	**Appl. Sure. Sci.** 2021, 560, 150036.
$BiVO_4/TiO_2$/ $NiCo_2O_4$	/	76%	**ACS Appl. Energy Mater.** 2020, 3, 5646
TiO_2/STO/CdS	32%	80%	**J. Mater. Chem. A** 2021, 9, 7594
TiO_2 nanotubes	1.7%	42.1%	**This work**
TiO_x-40	28.2%	89.0%	

Table S4 The relative concentration of oxygen vacancy obtained from XPS in Fig. 3.

Samples	Oxygen vacancy concentration Ov/O_{Ti-O} (%)
TiO_2	0
TiO_x-10	11.4
TiO_x-20	13.5
TiO_x-30	14.8
TiO_x-40	16.2
TiO_x-50	15.1

References

1. J. Tauc, R. Grigorovici and A. Vancu, *Phys. Status Solid.*, 1966, 15, 627–637.
2. Y. Zhang, Y. Tang, X. Liu, Z. Dong, H. H. Hng, Z. Chen, T. C. Sum and X. Chen, *Small*, 2013, 9, 996–1002.
3. B. Iandolo and A. Hellman, *Angew. Chem*., 2014, 126, 13622–13626.
4. Z. Chen, T. F. Jaramillo, T. G. Deutsch, A. Kleiman-Shwarsctein, A. J. Forman, N. Gaillard, R. Garland, K. Takanabe, C. Heske, M. Sunkara, E. W. McFarland, K. Domen, E. L. Miller, J. A. Turner and H. N. Dinh, *J. Mater. Res.*, 2011, 25, 3–16.
5. M. Ye, J. Gong, Y. Lai, C. Lin and Z. Lin, *J. Am. Chem. Soc.*, 2012, 134, 15720–15723.
6. W. Zhang, J. Xue, Q. Shen, S. Jia, J. Gao, X. Liu and H. Jia, *J. Alloys Compd.*, 2021, 870, 159400.
7. S. Wang, T. He, P. Chen, A. Du, K. Ostrikov, W. Huang and L. Wang, *Adv. Mater.*, 2020, 32, 2001385.